Chemical Geology 550 (2020) 119723

Contents lists available at ScienceDirect

Chemical Geology

journal homepage: www.elsevier.com/locate/chemgeo

Forearc origin for Coast Range Ophiolites inferred from osmium isotopes and highly siderophile elements

Eric Snortum, James M.D. Day*

Scripps Institution of Oceanography, La Jolla, CA 92093, USA

ARTICLE INFO

Editor: Balz Kamber

Keywords:
Ophiolite
Peridotite
Highly siderophile elements
Osmium
Mantle wedge
Forearc
Serpentinization

ABSTRACT

The Jurassic Coast Range Ophiolites, California, provide evidence for tectonic processes that formed the western margin of North America. Whether the ophiolites were formed in a mid-ocean ridge, back arc or forearc setting, however, remains unconstrained. To address this issue, a systematic grid sampling approach was taken to examine the mantle section of an archetypal ~161 Ma Coast Range Ophiolite at Point Sal, California. The Point Sal peridotites are serpentinized, with $^{187}Re-^{187}Os$ evidence for a localized Late Miocene alteration event in grids closest to the lowermost bounding fault of the ophiolite. This event is interpreted to be related to tectonic changes and hydration-dehydration reactions acting on the serpentinites in response to changes in the azimuth and rate of Pacific-North American plate motion. Alteration and serpentinization have not systematically affected highly siderophile element (HSE) abundances, especially Os, Ir or Ru which, together with rare earth element abundances, record significant melt depletion (> 20%) of a fertile mantle protolith ($^{187}Os/^{188}Os$ = ~0.129) during ophiolite formation. Peridotites subsequently experienced localized and heterogenous addition of Re, Pt, Pd and radiogenic $^{187}Os/^{188}Os$ from Cl-rich, oxidized (QFM) fluids. Geochemical features of both Point Sal peridotites, as well as associated basaltic lavas, are consistent with high degrees of partial melting and variable addition of fluids as also observed in global forearc peridotites. A forearc origin for the Point Sal Ophiolite Complex supports models for the dominant formation process of 153–166 Ma Coast Range Ophiolite infant Arc crust terranes within a single westward facing arc along the Sierra continental-margin.

1. Introduction

Mantle sections of obducted ophiolite complexes enable examination of mantle processes and provide evidence for the formation environment of the ophiolites themselves (e.g., Büchl et al., 2002; Kelemen et al., 1992; Schulte et al., 2009; Snow and Reisberg, 1995; O'Driscoll et al., 2012, 2015). Systematic grid sampling of ophiolite sections enables identification of melt refertilization and depletion processes, and the scale of mantle heterogeneity (O'Driscoll et al., 2018). Combined information for ophiolite mantle sections can therefore resolve petrogenetic processes and inform tectonic models, where ophiolites are obducted during subduction zone processes.

The California Continental Margin is a region where tectonic models for ophiolite formation remain contentious. Here, the Jurassic Coast Range Ophiolite (CRO) is a classic example for recent crust formation during arc processes ('infant Arc crust'; Fig. 1). Three contrasting hypotheses have been posited for CRO formation, involving formation in mid-ocean ridge settings, or within a forearc or back arc (Shervais and Kimbrough, 1985; Shervais, 1990; Stern and Bloomer, 1992). In general, supra-subduction zone type compositions of ophiolite rocks (e.g., Menzies et al., 1977; Shervais and Kimbrough, 1985; Shervais et al., 2004; Agranier et al., 2007; Choi et al., 2008), and paleomagnetic evidence for limited north-south movement, but potential east-west movement (Butler et al., 1991; Mankinen et al., 1991) suggest that back arc, intra-arc or forearc settings are most likely (Dickinson et al., 1996). A back arc or forearc origin, however, lead to contrasting models of California Continental Margin evolution. Back arc or intra-arc settings would require an east-facing arc that then collided with the west-facing Sierra continental-margin arc (Dickinson et al., 1996). A forearc origin requires the formation of the ophiolite in place within the west-facing arc-trench system lying along the continental margin.

To address the origin of the CRO, we document systematic grid sampling and geochemical analyses of serpentinized peridotites from the Point Sal Ophiolite Complex (PSOC). These data are used to identify serpentinization, alteration, melt infiltration and melt depletion processes during genesis of the PSOC mantle section and to explicitly

* Corresponding author.
E-mail address: jmdday@ucsd.edu (J.M.D. Day).

https://doi.org/10.1016/j.chemgeo.2020.119723
Received 14 April 2020; Received in revised form 5 June 2020; Accepted 7 June 2020
Available online 15 June 2020

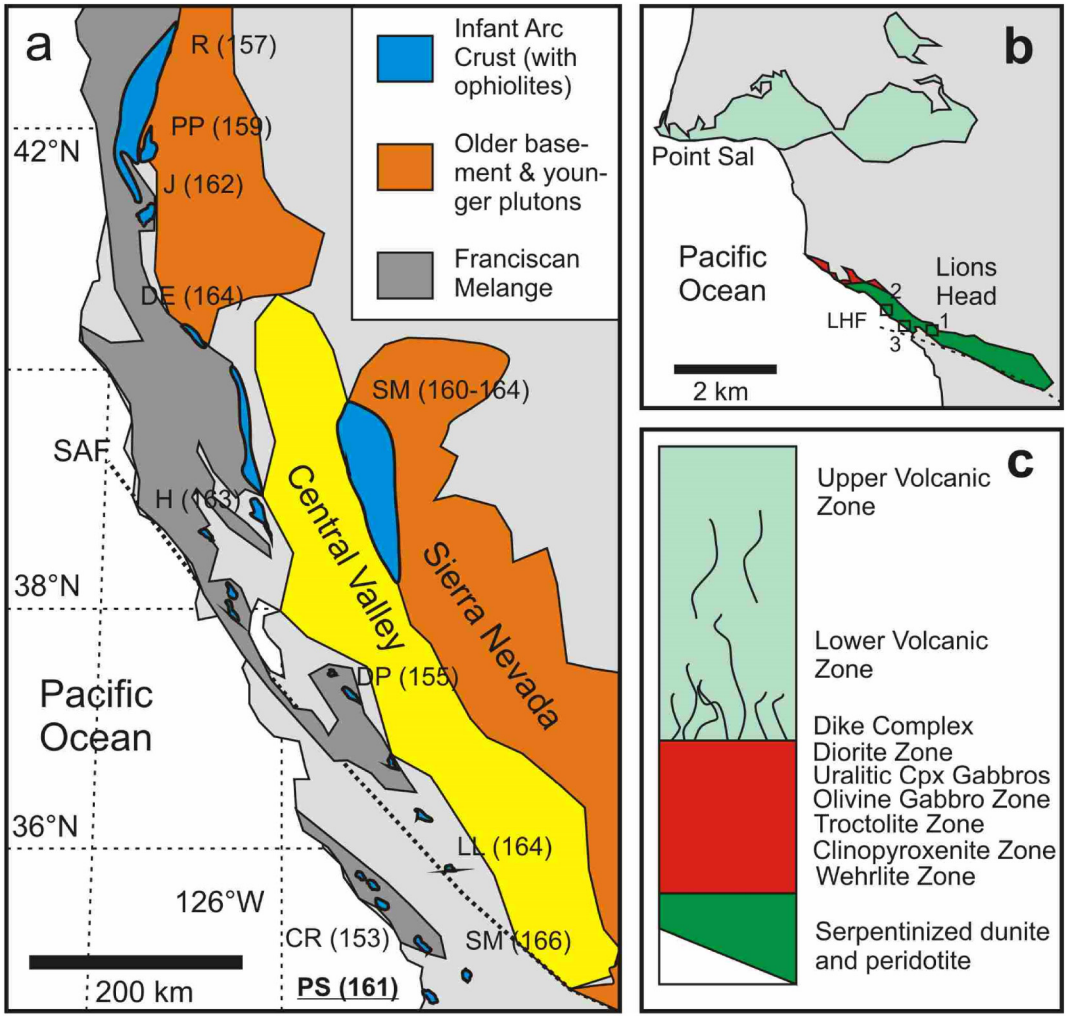

Fig. 1. (a) Map of Coast Range ophiolites and associated rocks, with average ages in parentheses, in millions of years. SAF = San Andreas Fault, and ophiolite complexes from S to N: PS = Point Sal Ophiolite Complex (PSOC); SM = Stanley Mountain; CR = Cuesta Ridge; LL = Llanada; DP = Del Puerto; H = Healdsburg; SM = Smartville; DE = Devil's Elbow; J = Josephine; PP = Preston Peak; R = Rogue Formation. (b) Map of PSOC, with unit colors described in (c) and younger cover shown in grey. Grid locations are given in (b). (c) idealized log through the ~3 km section of PSOC. Base is defined by the Lions Head Fault (LHF). Upper and lower volcanic zones are dominated by massive and pillowed submarine lavas. Map (a) modified from Stern and Bloomer (1992) and (b) and (c) adapted from Menzies et al. (1977).

examine the tectonic setting prior to and during emplacement.

2. Geological setting and methods

The Jurassic CRO in the California Coast Ranges comprises numerous deformed and structurally dismembered segments of oceanic crust and uppermost mantle incorporated into the continental margin (Bailey et al., 1970). Radiometric ages for igneous components of the ophiolites span from the Middle to Late Jurassic (~166 to ~153 Ma: Hopson et al., 1981; Saleeby et al., 1984; Mattinson and Hopson, 1992). The PSOC is considered one of the best-preserved ophiolites of the western margin of California (Dickinson et al., 1996). It is a ~161 Ma almost complete ophiolite, with serpentinized mantle peridotite, layered olivine and olivine-clinopyroxene ultramafic rocks, olivine and altered gabbro, diorite and quartz diorite, overlain by a dike complex and submarine lavas, with younger tuffaceous radiolarian cherts and shale (Hopson et al., 1975) (Fig. 1).

To examine the composition of the PSOC mantle section, we employed grid sampling at three locations within the serpentinized dunite and peridotite unit. Implicit bias in this approach is that an exposed outcrop needs to be chosen of sufficient size to accommodate a 3 × 2 m, 3 × 3 m, or larger grid, with grid sizes of 1 × 1 m. Samples were then collected as close to the center of the grid squares as possible, removing the issue of selective sampling within the grid (Supplementary Figs. S1–3). The advantage of this sampling technique, especially in altered peridotites is to remove the tendency to collect the 'freshest' samples, or to be drawn to unique or unusual features (c.f., O'Driscoll et al., 2018).

Large (> 2 kg) samples were collected, sawn, crushed and powdered prior to analysis for major- trace- (Table S1) and highly siderophile element (HSE) abundances and ^{187}Re—^{187}Os systematics (Table 1). In this contribution, general descriptions of samples and geochemical data are presented; future petrological information is desirable for detailed examination of siting of the HSE. Major element compositions were measured by X-ray fluorescence (XRF) at Franklin and Marshall College using a *PW 2404 PANalytical* XRF vacuum spectrometer following the procedures outlined in Boyd and Mertzman (1987). Major element analyses by XRF involved standard lithium tetraborate fusion techniques using 3.6:0.4 g $LiBO_4$:sample powder. Ferrous iron concentrations were determined by titration with potassium dichromate. Precision and accuracy are identical to those given previously in Day et al. (2017a).

Trace-element abundances were determined at the *Scripps Isotope Geochemistry Laboratory* (*SIGL*), Scripps Institution of Oceanography

Table 1
Rhenium-Os isotope and highly siderophile element abundance (in ppb) data for Point Sal peridotites.

Sample	MgO (wt%)	Al_2O_3 (wt%)	LOI (wt%)	Re	Pd	Pt	Ru	Ir	Os	$^{187}Re/^{188}Os$	2 St.Dev.	$^{187}Os/^{188}Os$	2 S.E.
PS1701A	41.1	0.90	14.5	0.152	12.05	8.982	0.906	0.848	0.285	2.523	0.038	0.13607	0.00024
PS1701B	42.1	0.84	14.5	0.016	9.371	33.21	1.132	2.121	0.290	0.258	0.004	0.13559	0.00018
PS1701C	42.7	0.84	15.1	0.047	3.041	3.653	0.961	0.529	0.272	0.824	0.012	0.14013	0.00023
PS1701D	42.2	0.87	14.9	0.021	5.942	4.810	0.567	0.615	0.095	1.037	0.016	0.15016	0.00039
PS1701E	41.7	0.25	14.8	0.027	10.75	2.516	0.375	0.391	0.075	1.711	0.026	0.15845	0.00041
PS1701F	42.5	0.94	15.2	0.023	7.588	7.872	0.710	0.995	0.155	0.694	0.010	0.14937	0.00027
PS1701G	41.4	0.66	15.6	0.101	7.089	10.21	0.718	0.818	0.180	2.657	0.040	0.13947	0.00023
PS1701H	40.0	1.27	15.6	1.594	7.928	7.528	0.687	0.747	0.151	50.2	0.8	0.14490	0.00028
PS1701I	42.3	0.38	14.9	0.468	8.288	18.68	0.930	0.922	0.214	10.3	0.2	0.13819	0.00024
PS1702A	46.9	0.49	15.9	0.042	1.976	6.341	1.896	1.557	0.672	0.293	0.004	0.12929	0.00095
PS1702B	47.5	0.78	18.0	0.032	4.846	19.28	1.917	0.792	0.770	0.199	0.003	0.12901	0.00012
PS1702C	47.6	0.64	16.9	0.053	3.060	5.674	2.087	0.681	0.743	0.341	0.005	0.12998	0.00020
PS1702D	47.7	0.68	16.9	0.026	2.824	7.677	1.667	0.792	0.472	0.264	0.004	0.12954	0.00018
PS1702E	46.9	1.38	17.2	0.072	9.186	10.02	1.892	1.313	1.055	0.324	0.005	0.12943	0.00013
PS1702F	46.9	1.20	18.0	0.050	0.982	1.530	1.730	0.510	0.502	0.476	0.007	0.12990	0.00017
PS1702G	47.3	0.81	18.0	0.040	3.234	4.864	2.453	1.083	0.752	0.252	0.004	0.12868	0.00013
PS1702H	46.7	0.81	17.9	0.029	2.285	31.17	2.247	1.321	0.673	0.201	0.003	0.12991	0.00027
PS1702I	47.4	0.71	18.0	0.050	2.418	3.051	1.691	0.597	0.429	0.549	0.008	0.13005	0.00020
PS1703A	39.1	4.47	13.9	1.106	3.076	1.258	1.377	0.397	0.930	5.6	0.1	0.13018	0.00013
PS1703B	40.5	3.54	14.0	0.140	3.923	3.556	1.341	0.616	0.754	0.881	0.013	0.13052	0.00014
PS1703C	48.6	0.22	17.5	0.068	0.234	0.530	0.790	0.138	0.233	1.381	0.021	0.12890	0.00023
PS1703D	45.1	0.88	15.3	1.548	0.709	0.632	1.678	0.593	0.554	13.2	0.2	0.13124	0.00017
PS1703E	45.4	2.00	15.9	0.211	34.67	1.618	1.015	0.201	0.277	3.602	0.054	0.12992	0.00021
PS1703F	43.2	2.69	14.8	0.126	1.145	1.121	6.530	2.028	2.664	0.224	0.003	0.12686	0.00011
MUH-1 Blk	Standard Reference Material			0.325	9.380	10.01	7.014	5.037	3.503			0.12724	0.00008
MUH-1 Blu	Standard Reference Material			0.204	11.77	7.970	8.472	3.717	5.311			0.12599	0.00008
MUH-1 Red	Standard Reference Material			0.215	9.721	6.916	9.767	3.740	4.688			0.12535	0.00008
MUH-1 Blk	Standard Reference Material			0.207	10.39	7.487	7.326	3.468	3.581			0.12687	0.00009

Uncertainty in $^{187}Re/^{188}Os$ reflects the propogated errors of the Os and Re abundance uncertainties. MUH-1 is a harzburgite standard reference material (see Meisel and Horan, 2016) and the colors (Blu = blue, Red, Blk = black) correspond measurements of aliquots from different vials of powder provided by T. Meisel.

using methods described previously (Day et al., 2017a). One hundred milligrams of powder was precisely weighed and digested in a 1:4 mixture of Teflon-distilled HNO_3:HF for > 72 Hrs at 150 °C on a hotplate. Rock standards (BHVO-2, BIR-1, HARZ-01, GP13) and total procedural blanks were prepared with samples. After drying down and sequential HNO_3 dry-down steps to break-down fluorides, clear sample solutions, free of any solid material, were diluted in two sets. The first set was diluted by a factor of 5000 in 2% HNO_3 for all trace element determinations. The second set was diluted by a factor of 1000 for rare earth element determination. Both sets of solution were doped with a 1 ppb In solution to monitor instrumental drift. Solutions were measured using a *Thermo Scientific* iCAP Qc quadrupole inductively coupled plasma mass spectrometer at the *SIGL*. Reproducibility of the basaltic reference materials were better than 5% (RSD), whereas the reproducibility of measurements for harzburgite reference material, HARZ-01 and peridotite GP-13 were between 5 and 20% (RSD), with element abundances within error of recommended values (see also Day et al., 2017a; Snortum et al., 2019).

Osmium isotope and HSE abundance analyses were performed at the *SIGL*. One gram of homogenized powder was precisely weighted before digestion in sealed borosilicate Carius tubes with isotopically enriched multi-element spikes (^{99}Ru, ^{106}Pd, ^{185}Re, ^{190}Os, ^{191}Ir, ^{194}Pt), and 12 mL of a 1:2 mixture of multiply Teflon distilled HCl and HNO_3 purged of excess Os by repeated treatment and reaction with H_2O_2. Samples were digested to a maximum temperature of 270 °C in an oven for 72 h. Osmium was triply extracted from the acid using CCl_4 and then back extracted into HBr (Cohen and Waters, 1996), prior to purification by micro-distillation (Birck et al., 1997). Rhenium and the other HSE were recovered and purified from the residual solutions using standard anion exchange separation techniques (Day et al., 2016).

Isotopic compositions of Os were measured in negative-ion mode using a *ThermoScientific* Triton thermal ionization mass spectrometer in peak-jumping mode on the secondary electron multiplier. Rhenium, Pd, Pt, Ru and Ir were measured using a *Cetac Aridus II* desolvating nebuliser coupled to a *ThermoScientific* iCAPQc ICP-MS. Offline corrections for Os involved an oxide correction, an iterative fractionation correction using $^{192}Os/^{188}Os = 3.08271$ and assuming the exponential law, a ^{190}Os spike subtraction, and an Os blank subtraction. Precision for $^{187}Os/^{188}Os$, determined by repeated measurement of the UMCP Johnson-Matthey standard was better than ± 0.2% (2 SD; 0.11374 ± 8; n = 6). Rhenium, Ir, Pt, Pd and Ru isotopic ratios for sample solutions were corrected for mass fractionation using the deviation of the standard average run on the day over the natural ratio for the element. External reproducibility for HSE analyses was better than 0.5% for 0.5 ppb solutions and all reported values are blank corrected. The total procedural blanks (n = 2) run with the samples gave $^{187}Os/^{188}Os = 0.183 \pm 0.006$, with quantities (in picograms) of 3 to 6 [Re], 21 [Pd], 3 [Pt], 51 to 59 [Ru], 12 to 15 [Ir] and 0.3 to 0.5 [Os]. These blanks resulted in negligible corrections to samples (< 5%) except for blank additions PS1703C (up to 25% for Pd; Table S2). A peridotite standard, MUH-1 was run with samples four times during the analytical campaign (see also Snortum et al., 2019), and concentrations and isotopic compositions for this standard reference material are within uncertainty of a larger suite of measurements made using both Carius tube and high-pressure asher digestion methods (Meisel and Horan, 2016). Blue, black and red data reported in Table S1 refer to the different aliquots of MUH-1 provided by T. Meisel.

3. Results

Samples from all three grids are serpentinites from peridotite protoliths with elevated LOI-corrected MgO contents (39–47 wt%), low Na_2O, K_2O and P_2O_5, and variable CaO and Al_2O_3 (0.25–4.5 wt%). All samples have loss on ignition (LOI) exceeding 13.9 wt%, with the extent of LOI for grids occurring in the order PS1702 (> 15.9 wt %) > PS1703 ≥ PS1701. High Mg-numbers (73–80) and Cr contents (1425–22,400 ppm) indicate that the unaltered protoliths to samples were Cr-spinel bearing dunite or harzburgite. There are no correlations with HSE compositions and LOI (Fig. 2). Incompatible trace element (ITE) abundances are generally depleted, having equal or lower

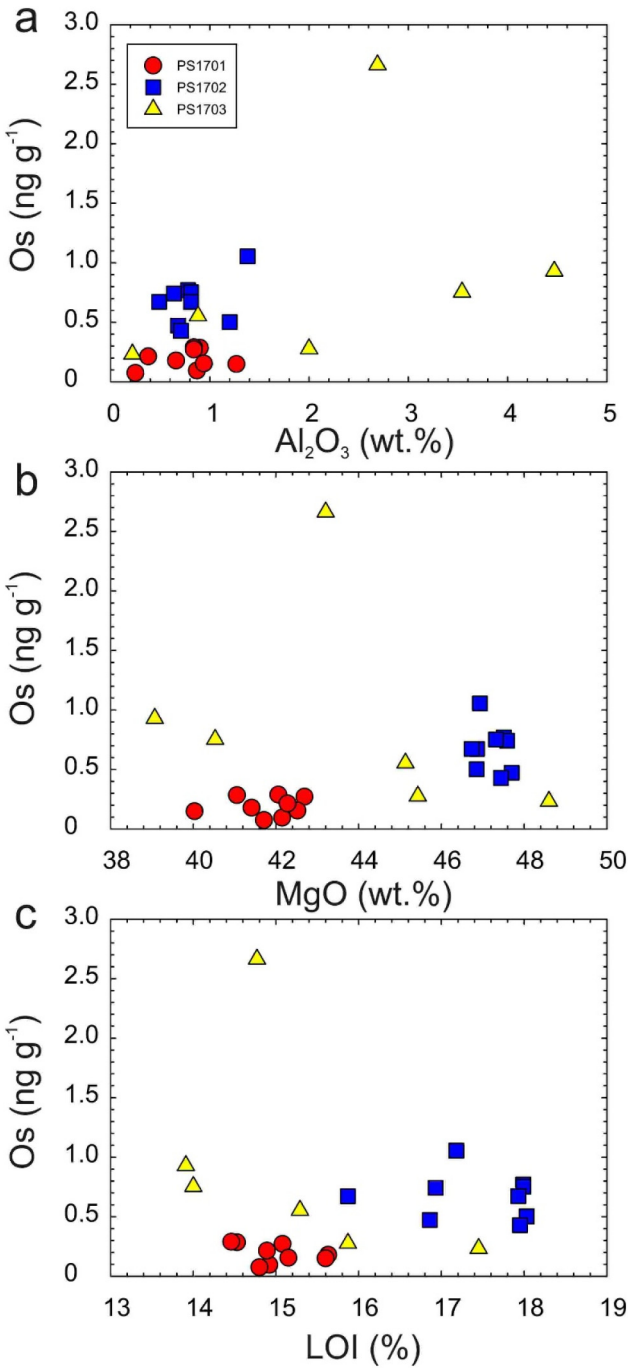

Fig. 2. Plots of osmium content versus (a) Al_2O_3, (b) MgO and (c) loss on ignition (LOI) for Point Sal Ophiolite Complex serpentinites.

abundances than in the most depleted abyssal peridotites. Trace element enrichment or depletion relative to the primitive mantle (PM) composition vary, with grid PS1702 being generally the most depleted and PS1701 being the most enriched. All samples have relative enrichments in Ba, U, Sr and Ti, and depletion in Th. While samples are generally strongly depleted in the heavy rare earth elements (HREE; < 1 to 0.01 × chondrite) they do not exhibit the light REE depletion of some abyssal peridotites (Fig. 3).

Highly siderophile element (HSE) contents of PSOC samples are both distinct between grids and from the PM composition (Fig. 3; Table 1). Samples have Os, Ir and Ru contents lower than PM abundances, with variable Ir/Os between grids (PS1701 = ~4.9; PS1702 = ~1.4; PS1703 = ~0.7). Osmium, Ru and, to a lesser extent

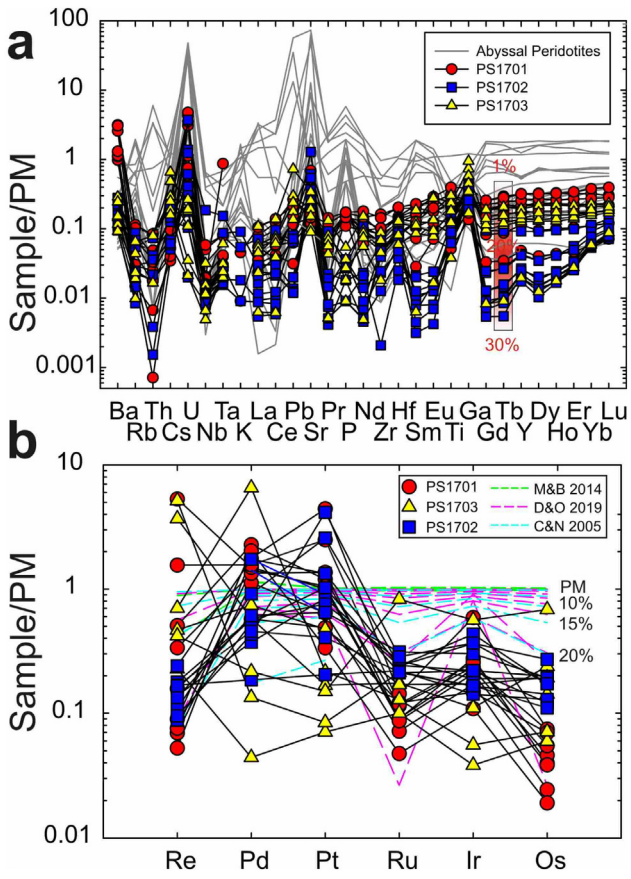

Fig. 3. (a) Primitive mantle (PM)-normalized incompatible trace element diagram for Point Sal Ophiolite Complex rocks compared with abyssal peridotites (Day et al., 2017a). Percent partial melting estimates for Tb are given from the melt model described in the text. PM normalization from McDonough and Sun (1995). **(b)** Primitive mantle normalized highly siderophile element patterns for PSOC grids. Shown are melt-depletion models in 5% melt loss increments using three different sulfide/silicate *D* values from Chazey and Neal (2005) (C&N), Mungall and Brenan (2014) (M&B), Day and O'Driscoll (2019) (D&O) using primitive mantle compositions given in Day et al. (2017a).

Ir, correlate positively with Cr content, indicating that these elements are likely to be primarily hosted with Cr-spinel in the serpentinites. Platinum and Pd are generally elevated in grids PS1701 and PS1702, and more variable in PS1703 (Pt/Os for PS1701 = ~54; PS1702 = ~14.5; PS1703 = ~2.6). Rhenium, Pt and Pd are uncorrelated with Cr content. Rhenium contents vary considerably in PS1701 and PS1703, but show a limited range in PS1702 (0.03–0.07 ppb). Consequently, while $^{187}Re/^{188}Os$ spans a limited range in PS1702 (0.2–0.55), the other grids extend to more extreme ratios (0.22–50). Grid PS1702 exhibits a limited range in $^{187}Os/^{188}Os$ (0.1287–0.1301; mean = 0.1295 ± 10; 2SD), followed by PS1703 (0.1269–0.1312; mean = 0.1296 ± 31), with PS1701 being both the most radiogenic with respect to $^{187}Os/^{188}Os$, with the greatest range of isotopic compositions (0.1356–0.1585; mean = 0.144 ± 16).

4. Discussion

4.1. Timing and extent of modification processes

The PSOC mantle section is variably serpentinized, and while serpentinization processes can have a strong control on some incompatible trace elements (e.g., B, U, Sr, Ba, Pb; Table S1), they have more limited effect on REE abundances, as also observed for other serpentinized peridotites (e.g., Allen and Seyfried, 2005; Paulick et al., 2006;

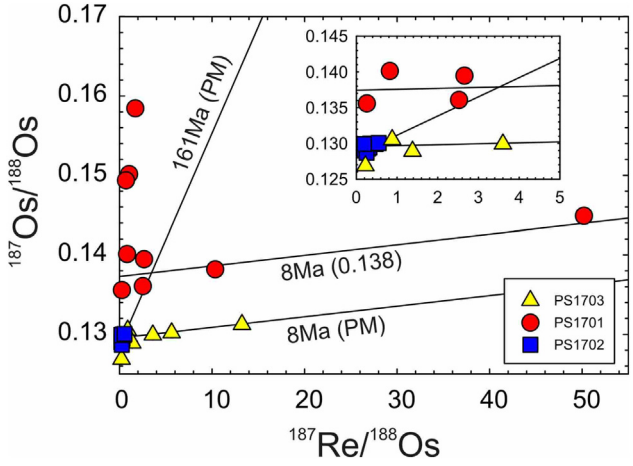

Fig. 4. $^{187}Re/^{188}Os$-$^{187}Os/^{188}Os$ systematics for the Point Sal Ophiolite Complex. Inset gives expanded view for samples with $^{187}Re/^{188}Os$ from zero to 5. Isochron lines are for primitive mantle composition at the inferred age of ophiolite formation (161 Ma PM) and 8 Ma, in response to Late Miocene plate reconfiguration (e.g., Atwater and Stock, 1998) with PM and a more radiogenic initial value (0.138) at that time.

Kodolányi et al., 2012). Instead, the REE variations in the samples are consistent with PSOC mantle that experienced melt depletion followed by minor refertilization. Different grids show variable extents of melt refertilization. All grid samples have a similar range of Ti contents (46–476 ppm), whereas PS1702 has the greatest REE depletion, with PS1701 and PS1703 being similarly relative enriched compared to PS1702, with generally elevated light REE and large ion lithophile element abundances (Fig. 3). The depletion in the REE provides strong evidence for moderate to extensive melt depletion.

Abundances of the HSE (Os, Ir, Ru, Pt, Pd) and $^{187}Os/^{188}Os$ are uncorrelated with indicators of serpentinization, with grids with the highest LOI having variable HSE abundances and isotopic compositions. Grid PS1702 samples cluster along a 161 Ma PM isochron on a $^{187}Re/^{188}Os$-$^{187}Os/^{188}Os$ diagram, implying a fertile mantle source at the time of PSOC formation (Fig. 4). Grid PS1703 samples also have PM-like $^{187}Os/^{188}Os$ but extend to higher $^{187}Re/^{188}Os$ and conform to a young apparent age (~8 Ma). Grid PS1701 has the most radiogenic $^{187}Os/^{188}Os$ and some samples also have high $^{187}Re/^{188}Os$ (> 5) that fall along a similarly young apparent age as samples in PS1703.

The Os isotope systematics for PS1701 and PS1703, grids which are closest in proximity to the bounding Lions Head Fault, can be accounted for by Late Miocene addition of Re that consequently led to recent in-growth of ^{187}Os, superimposed on variable initial $^{187}Os/^{188}Os$ between grids. The lower LOI contents, enhanced ITE abundances and ^{187}Re–^{187}Os systematics of grids PS1701 and PS1703 all imply heating and fluid-exchange processes led to modification. Plate reconstruction models suggest that at about 8 Ma, the azimuth and rate of Pacific-North American plate motion changed (e.g., Atwater and Stock, 1998). We therefore suggest that Late Miocene structural and modification, particularly proximal to the Lions Head Fault, and associated hydration-dehydration reactions in the serpentinites, led to modification of portions of PSOC peridotite.

Previous studies have suggested that $^{187}Os/^{188}Os$ can be modified by hydrothermal alteration and sea-floor weathering (e.g., Snow and Reisberg, 1995). It is not clear if the serpentinization of the PSOC was solely due to seawater hydrothermal alteration given its setting and a complex heritage of emplacement into the California Continental Margin. However, if serpentinization was controlled by this process, LOI and other indicators of alteration with HSE contents and Os isotopic compositions are uncorrelated. These lines of evidence indicate that bulk-rock PSOC compositions predominantly reflect their high temperature mantle petrogenesis rather than variations due to hydrothermal alteration or high fluid/rock ratios. This is consistent with preservation of mantle peridotite Os isotope and HSE abundances even in steatized talc-magnesite samples (LOI = ~20 wt%) formed as peridotites within the Shetland Ophiolite Complex (Day et al., 2017b). From a geochemical perspective, data from the PSOC grids confirm prior work that has shown that, while serpentinization can result in some modification to HSE abundances and Os isotope systematics, it does not obscure prior melt depletion or refertilization, enabling assessment of mantle processes even in strongly serpentinized rocks (e.g., Liu et al., 2008; Day et al., 2017a, 2017b). In the case of the PSOC, neither melt refertilization nor alteration processes provide satisfactory explanations for the variable $^{187}Os/^{188}Os$ between grids, or their variable Ir/Os and high Pt and Pd contents.

4.2. Evidence for fluid-assisted melting

Peridotite samples from the PSOC have experienced significant melt depletion evident from high MgO, low Al_2O_3, and low heavy REE abundances, especially for grids PS1701 and PS1702. Two melt depletion estimates are presented, using rare earth element (REE) and HSE abundances (Fig. 3). The REE depletion model employs the starting composition of depleted MORB mantle (DMM) from Workman and Hart (2005), and partition coefficients (*D* values) for olivine, orthopyroxene, clinopyroxene and spinel from Suhr et al. (1998) and Sun and Liang (2014) and has previously been presented in Day et al. (2017a). To assess HSE depletion, a non-modal fractional melting model was used with three sulfide/silicate *D* values, as also previously employed in Day et al. (2017a). These models are reliant on the exhaustion of S, which we assume to initially be ~250 ppm (McDonough and Sun, 1995), given the primitive mantle-like initial Os isotope compositions of PSOC peridotites. A set of *D* values were obtained from the experiments of Mungall and Brenan (2014), with the other two datasets from empirical estimates from basalts and layered intrusions from Chazey and Neal (2005) and Day and O'Driscoll (2019), respectively (Fig. 3).

The REE data for grids PS1701 and PS1703 can be explained by 20% partial melting in the most depleted samples, with PS1702 samples requiring > 20% partial melting. Relationships of Ti-V-Yb in samples from the grids imply relatively shallow partial melting occurred under oxidized conditions (QFM) in the spinel stability field (Fig. 5). Models of melt depletion for the HSE using the observed *D*-values conform quite well with > 20% partial melting inferred for all three grids. In contrast, experimentally derived *D*-values from Mungall and Brenan (2014) do not reproduce melt depletion, requiring > 30% partial melting for all grids. All three *D*-values predict significant Ir/Os fractionation at high degrees of melt loss, which are evident in data for PS1701 and PS1702. This significant fractionation is due to the progressive exhaustion of sulfur in the source during melting, leading to preferential loss of Os and Ru from Ir, likely during alloy stabilization (e.g., Kepezhinskas and Defant, 2001; Lorand and Luguet, 2016; O'Driscoll and González-Jiménez, 2016).

Since Os and Ru are well correlated with Cr, whereas Ir is less well correlated, it is likely that these elements now occur associated with spinel and alloys, respectively. Since $^{187}Os/^{188}Os$ correlates negatively with Os content in PSOC samples, the Os hosted with Cr-spinel is also relatively unradiogenic and suggests a similar mantle source composition (≤0.129) for all grids. Melt depletion cannot explain the high Pt and Pd contents observed in these grids, or the variable $^{187}Os/^{188}Os$ between the grids, where melt depletion is expected to generate low Re/Os. The primitive mantle-like $^{187}Os/^{188}Os$ of PS1702 and PS1703 samples imply melt depletion occurred during formation of the PSOC rather than in any prior events, as has been observed for modern Pacific mantle lithosphere (Snortum et al., 2019). This observation would imply that the mantle protolith to the PSOC was relatively homogeneous in composition. For example, $^{187}Os/^{188}Os$ of PS1701 samples correspond to the lowest Os contents of all PSOC peridotites and indicate addition of a radiogenic ^{187}Os melt or fluid component following

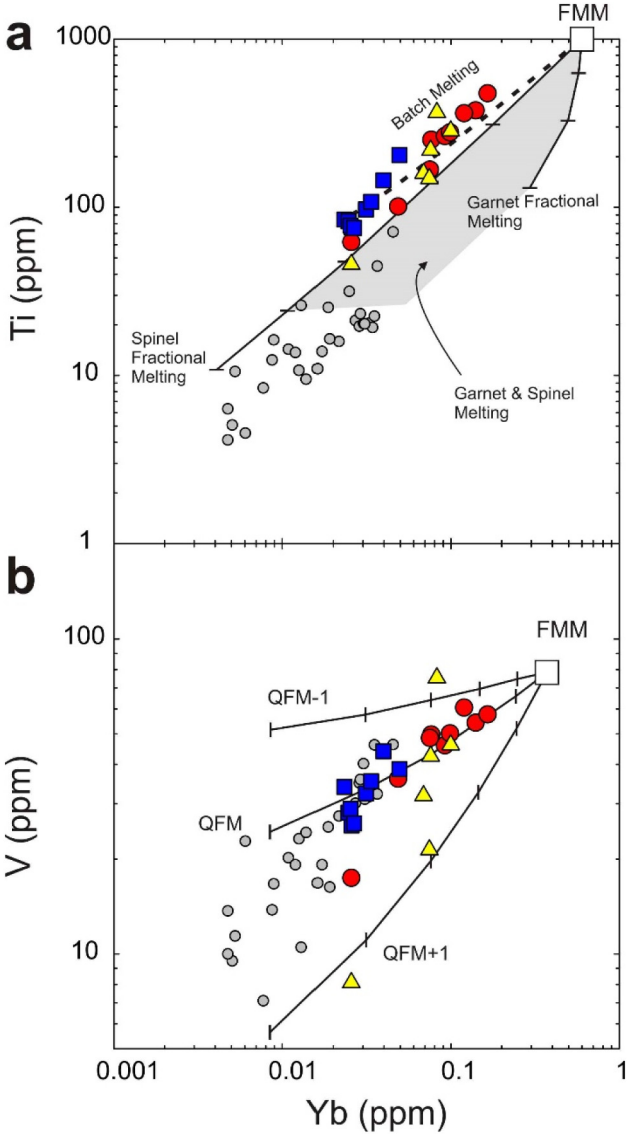

Fig. 5. Plots of Ti versus Yb and V versus Yb for PSOC peridotites. The modelled melt extraction and oxygen fugacities (quartz-magnetite-fayalite [QFM] buffer) are from Pearce and Parkinson (1993) and Parkinson and Pearce (1998). The theoretical composition of fertile MORB mantle is shown as FMM (Pearce and Parkinson, 1993). The grey filled symbols are compositions of peridotites from the Izu-Bonin-Mariana forearc Parkinson and Pearce (1998). In the spinel stability field, both Ti and Yb are incompatible. In the garnet stability field, extraction of Yb into the melt is suppressed relative to Ti, because of its favorable incorporation into garnet such that it behaves instead as a slightly incompatible, or even compatible element. Pearce and Parkinson (1993) and Parkinson and Pearce (1998) also used bivariate plots of V versus Yb in order to assess fO_2 conditions during mantle melting. In mid-ocean ridge settings (~QFM-1; quartz-fayalite-magnetite buffer), V behaves as a moderately incompatible element, whereas under the more oxidizing conditions that may obtain occur during SSZ melting of peridotites modified by aqueous fluids rising from the down-going slab (~QFM), V acts as a highly incompatible trace element. Symbols for PSOC peridotites are the same as for Fig. 4.

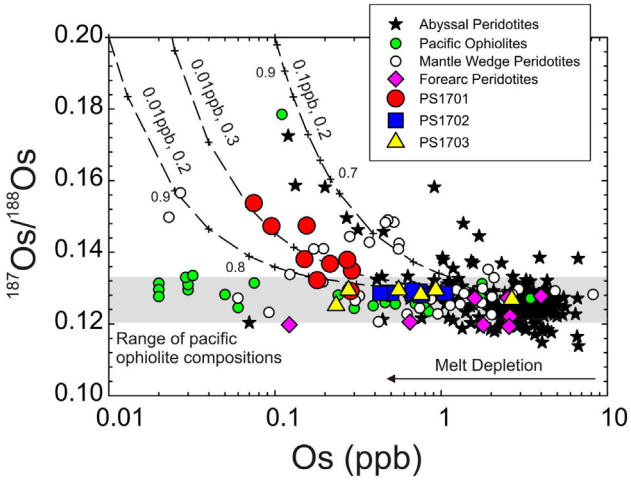

Fig. 6. Osmium versus $^{187}Os/^{188}Os$ for PSOC serpentinites compared with abyssal peridotites (Day et al., 2017a), fore-arc ophiolites (McInnes et al., 1999; Liu et al., 2018), fore-arc peridotites (Parkinson et al., 1998) and mantle wedge peridotite xenoliths (Brandon et al., 1996; Widom et al., 2003; Saha et al., 2005). Models show mixing between PM ($^{187}Os/^{188}Os$ = 0.129; Os = 3 ppb) and variable fluid compositions (concentration and $^{187}Os/^{188}Os$) shown on the figure with crosses in 5% increments. Samples in grid PS1701 requires significant melt depletion and ~ two times greater addition of ^{187}Os-rich fluids compared with PS1702 or PS1703, consistent with their Os, Ir and Ru poor, but incompatible element and Pt and Pd enriched character. Similar ^{187}Os-rich fluid addition occurs, albeit with heterogeneous distribution, in some mantle wedge peridotites.

extensive (> 20%) partial melt depletion of this relatively homogeneous mantle source.

Differences in HSE contents and Os isotope compositions between grids PS1701 and PS1702 can be used to constrain likely compositions of melt or fluid addition. Although such models are non-unique, the compositions of Grid PS1701 samples can be explained by up to two times more addition of a fluid with moderately radiogenic $^{187}Os/^{188}Os$ (0.2–0.3) and variably low Os contents (0.01–0.1 ppb Os) to explain deviations from PS1702, as illustrated in the models in Fig. 6. To perturb the $^{187}Os/^{188}Os$ of PS1702 and PS1703 would therefore requires higher fluid addition, or a fluid with higher Os content. Radiogenic $^{187}Os/^{188}Os$ and low Os peridotites also occur for mantle wedge xenoliths. In order to explain the enrichments in Pd and Pt requires that the same fluid composition would have high Re (5 ppb), Pt and Pd (100 ppb). A possible source of high Pt, Pd, Re and radiogenic $^{187}Os/^{188}Os$ would be dissolution of Pd, Pt rich sulfides, such as pentlandite in percolating oxidized fluids or melts. It has been proposed that low Pd/Ir in recycled oceanic crust is due to dissolution and loss of Pd-rich species, including pentlandite (Dale et al., 2009). This is consistent with both high degrees of partial melting to explain low HSE contents in forearc peridotites with unradiogenic $^{187}Os/^{188}Os$ (Parkinson et al., 1998; Liu et al., 2018), and the radiogenic $^{187}Os/^{188}Os$ in sub-arc mantle wedge peridotites through subsequent fluid addition (Brandon et al., 1996; Saha et al., 2005; Widom et al., 2003). Experimental data (Xiong and Wood, 2000; Righter et al., 2002) has been used to propose that the radiogenic ^{187}Os originates from slab derived Cl-rich, oxidized fluids, where there is increasing solubility of Os. In the case of the PSOC, fluid enhanced partial melting explains the levels of melt depletion (> 20%), with late refertilization through heterogeneous distribution of radiogenic and oxidized (QFM) slab-derived fluids.

4.3. Grid sampling in peridotite complexes

Study of the PSOC exemplifies the utility of grid sampling in ophiolite complexes, as has previously been shown by O'Driscoll et al. (2018) for the Shetland Ophiolite Complex. Grid sampling at three locations within the PSOC mantle section has outlined both consistency (PS1701, PS1702) and variability (PS1703) in major elements between grids, differences in trace element compositions within and between grids, and a lack of coherent variability between the HSE and indicators of serpentinization (LOI) in the PSOC. Perhaps most significantly, the grids closest to the lowermost bounding fault of the PSOC (the Lions Head Fault) show evidence for Late Miocene fluid alteration, affecting

$^{187}Re-^{187}Os$ systematics. Age-corrected $^{187}Os/^{188}Os$ versus Os contents for the grids also show that PS1701 samples experienced significant fluid addition during formation of the ophiolite.

Without the systematic grid sampling, it is difficult to envisage how these conclusions would have been borne out for the PSOC. For example, randomly selecting six or ten samples from the three grids, assuming a similar sampling density to that previously applied in many ophiolite complexes, does not lead to the same conclusions without serendipity. In particular, it would be difficult to recognize the Late Miocene event observed in PS1701 and PS1702. Another example is the localized effect of radiogenic fluid addition that affected PS1701 samples, but not PS1702 or PS1703 samples, during formation of the ophiolite. Liu et al. (2018) used peridotite boulders collected from streams in the New Caledonia forearc ophiolite to propose that stability of sulfide at different depth may explain differences in forearc peridotites in terms of radiogenic ^{187}Os originating from slab derived Cl-rich, oxidized fluids. Due to grid sampling, it is possible to rule out this possibility for the PSOC, where the sampling grids are less than a kilometer apart. Instead, the data requires a heterogeneous distribution of radiogenic and oxidized (QFM) slab-derived fluids, where only peridotites in grid PS1701 were significantly affected by this process. A heterogeneous distribution of radiogenic and oxidized slab-derived fluids may also be a more effective model for understanding Os isotopic heterogeneity in mantle wedge and forearc peridotites in general.

The grid sampling that we employed and that enabled recognition of the aforementioned processes was 1 × 1 m sized boxes within 3 × 3 or 3 × 2 m grids. Arguably, a mixture of 1 m grid sampling, combined with small-scale grids (< 1 m grids) and systematic sampling at 5 to 100 m distances within peridotite massifs and ophiolite complexes may be useful for deconvolving large-scale processes from small-scale heterogeneities introduced from localized melting, fluid-flow and addition and late-stage processes, to more quantitatively examine the nature of upper mantle processes.

4.4. A fore-arc setting for the Jurassic Coast Range Ophiolites

There is debate regarding the origin of the CRO. Three models have been proposed: (1) a back-arc or intra-ocean island arc origin; (2) genesis at a mid-ocean ridge and (3) formation in a forearc setting (Dickinson et al., 1996). In the case of (1) and (3), an origin associated with subduction is required. In the case of (2) and (3) only a single facing Sierra magmatic arc is required, whereas (1) requires an east facing arc to explain the ophiolite distribution in the CRO. Models (1) and (2) typically suggest less fluid-assisted melting than (3). Finally, models (1) and (2) both require tectonic transport of the ophiolite to the continental margin, whereas model (3) requires formation of the ophiolite in place within an arc-trench system lying along the continental margin. The PSOC allows resolution of this debate. The previously reported geochemistry of PSOC lavas demonstrate the lowest basalts are similarly REE depleted to MORB, whereas upper basaltic lavas are strongly REE depleted (Menzies et al., 1977). PSOC peridotites and lavas indicate significantly greater melt-depletion than would be expected in mid-ocean ridge or in back arc or intra-oceanic island arc settings. A mid-ocean ridge origin (model 2) for the PSOC can be categorically discounted based on the high degrees of partial melting and melt depletion that the peridotites experienced at the time of ophiolite formation. Instead, the high degree of partial melting and existence of oxidized (QFM), radiogenic ^{187}Os and high Pt and Pd fluids are most consistent with a forearc, high-water flux origin for the PSOC. Our results support recent models whereby the CRO is dominantly formed through subduction processes (e.g., Choi et al., 2008), followed by collision of an active spreading ridge (Shervais et al., 2004). Ultimately, the geographic location of the PSOC within the western edge of the CRO, and the limited range in ages and supra-subduction zone compositions of CRO complexes (e.g., Agranier et al., 2007; Choi et al., 2008; Jean et al., 2010; Barnes et al., 2013; Wakabayashi, 2017) indicate that a forearc origin is the most likely origin for Sierra infant arc crust.

5. Conclusions

Systematic grid sampling of the mantle section of the ~161 Ma Point Sal Ophiolite Complex (PSOC) enables separation of Late Miocene, tectonically mediated alteration of serpentinized peridotites and serpentinization processes from fluid-driven refertilization and melt-depletion processes during formation of the ophiolite itself. During formation of the ophiolite, the mantle section experienced > 20% partial melting and significant depletion of Os, Ir and Ru during exhaustion of sulfide. Succeeding or concomitant with this process, distinct portions of the ophiolite mantle section experienced infiltration by oxidized Cl-rich fluids from the break-down of radiogenic, Pt and Pd-rich sulfides, suggesting heterogeneous fluid-flow within the mantle section. Combined with the high-depleted compositions of associated submarine lavas in the PSOC (Menzies et al., 1977), the results point to formation in a supra-subduction zone environment with significant fluid-assisted melting and associated formation of oxidized fluids. Such conditions are inconsistent with a mid-ocean ridge setting, and most consistent with a forearc setting, rather than a back arc setting, given the high fluid flow and degrees of partial melting (> 20%) required. With the similarity in setting determined for other CRO complexes, our results strongly implicate a forearc origin as the most likely origin for Sierra infant arc crust and a single westward facing arc in the Jurassic along the west coast of North America.

Supplementary data to this article can be found online at https://doi.org/10.1016/j.chemgeo.2020.119723.

Declaration of competing interest

The authors declare that they have no known competing financial interests or personal relationships that could have appeared to influence the work reported in this paper.

Acknowledgements

We thank T. Curry-Bumpass and Vandenburg Air Force Base for access, M. Menzies and C. Hopson for information on Point Sal, and B. Oller for suggestions. Comments from J. Kodolányi and an anonymous reviewer, and editorial handling by B. Kamber are greatly appreciated. This work was supported by the National Science Foundation (NSF EAR 1447130 and 1918322).

References

Agranier, A., Lee, C.T.A., Li, Z.X.A., Leeman, W.P., 2007. Fluid-mobile element budgets in serpentinized oceanic lithospheric mantle: insights from B, As, Li, Pb, PGEs and Os isotopes in the Feather River Ophiolite, California. Chem. Geol. 245, 230–241.

Allen, D.E., Seyfried Jr, W.E., 2005. REE controls in ultramafic hosted MOR hydrothermal systems: an experimental study at elevated temperature and pressure. Geochim. Cosmochim. Acta, 69, pp. 675–683.

Atwater, T., Stock, J., 1998. Pacific-North America plate tectonics of the Neogene southwestern United States: an update. Int. Geol. Rev. 40, 375–402.

Bailey, E.H., Blake Jr., M.C., Jones, D.L., 1970. On-Land Mesozoic Ocean Crust in California Coast Ranges: U.S. Geological Survey Professional Paper 700-C. pp. C70–C81.

Barnes, J.D., Eldam, R., Lee, C.T.A., Errico, J.C., Loewy, S., Cisneros, M., 2013. Petrogenesis of serpentinites from the Franciscan Complex, western California, USA. Lithos 178, 143–157.

Birck, J.L., Barman, M.R., Capmas, F., 1997. Re-Os isotopic measurements at the femtomole level in natural samples. Geostand. Geoanal. Res. 21, 19–27.

Boyd, F.R., Mertzman, S.A., 1987. Composition and structure of the Kaapvaal lithosphere, southern Africa. In: Magmatic Processes: Physicochemical Principles. 1. pp. 3–12.

Brandon, A.D., Creaser, R.A., Shirey, S.B., Carlson, R.W., 1996. Osmium recycling in subduction zones. Science 272, 861–863.

Büchl, A., Brügmann, G., Batanova, V.G., Münker, C., Hofmann, A.W., 2002. Melt percolation monitored by Os isotopes and HSE abundances: a case study from the mantle section of the Troodos Ophiolite. Earth Planet. Sci. Lett. 204, 385–402.

Butler, R.F., Dickinson, W.R., Gehrels, G.E., 1991. Paleomagnetism of coastal California

and Baja California: Alternatives to large-scale northward transport. Tectonics 10, 561–576.
Chazey, W.J., Neal, C.R., 2005. Platinum-group element constraints on source composition and magma evolution of the Kerguelen Plateau using basalts from ODP Leg 183. Geochim. Cosmochim. Acta 69, 4685–4701.
Choi, S.H., Shervais, J.W., Mukasa, S.B., 2008. Supra-subduction and abyssal mantle peridotites of the Coast Range ophiolite, California. Contrib. Mineral. Petrol. 156, 551.
Cohen, A.S., Waters, F.G., 1996. Separation of osmium from geological materials by solvent extraction for analysis by thermal ionisation mass spectrometry. Anal. Chim. Acta 332, 269–275.
Dale, C.W., Burton, K.W., Pearson, D.G., Gannoun, A., Alard, O., Argles, T.W., Parkinson, I.J., 2009. Highly siderophile element behaviour accompanying subduction of oceanic crust: whole rock and mineral-scale insights from a high-pressure terrain. Geochim. Cosmochim. Acta 73, 1394–1416.
Day, J.M.D., O'Driscoll, B., 2019. Ancient crustal contaminants with high Pt/Os can explain radiogenic ^{186}Os in intraplate magmas. Earth Planet. Sci. Lett. 519, 101–108.
Day, J.M.D., Waters, C.L., Schaefer, B.F., Walker, R.J., Turner, S., 2016. Use of hydrofluoric acid desilicification in the determination of highly siderophile element abundances and Re-Pt-Os isotope systematics in mafic-ultramafic rocks. Geostand. Geoanal. Res. 40, 49–65.
Day, J.M.D., Walker, R.J., Warren, J.M., 2017a. ^{186}Os-^{187}Os and highly siderophile element abundance systematics of the mantle revealed by abyssal peridotites and Os-rich alloys. Geochim. Cosmochim. Acta 200, 232–254.
Day, J.M.D., O'Driscoll, B., Strachan, R.A., Daly, J.S., Walker, R.J., 2017b. Identification of mantle peridotite as a possible Iapetan ophiolite sliver in south Shetland, Scottish Caledonides. J. Geol. Soc. Lond. 174, 88–92.
Dickinson, W.R., Hopson, C.A., Saleeby, J.B., 1996. Alternate origins of the Coast Range ophiolite (California): introduction and implications. GSA Today 6, 1–10.
Hopson, C.A., Frano, C.J., Pessagno, E.A., Mattinson, J.M., 1975. Preliminary Report and Geologic Guide to the Jurassic Ophiolite near Point Sal, Southern California Coast, Prepared for the 71 St Annu. Meet. Geol. Soc. Am.
Hopson, C. A., Mattinson, J. M., Pessagno, E. A., Jr., 1981, Coast Range Ophiolite, western California, in Ernst, W. G., ed., The Geotectonic Development of California: Englewood Cliffs, New Jersey, Prentice-Hall, p. 418–510.
Jean, M.M., Shervais, J.W., Choi, S.H., Mukasa, S.B., 2010. Melt extraction and melt refertilization in mantle peridotite of the Coast Range ophiolite: an LA–ICP–MS study. Contrib. Mineral. Petrol. 159, 113.
Kelemen, P.B., Dick, H.J.B., Quick, J.E., 1992. Formation of harzburgite by pervasive melt/rock reaction in the upper mantle. Nature 358, 635–641.
Kepezhinskas, P., Defant, M.J., 2001. Nonchondritic Pt/Pd ratios in arc mantle xenoliths: evidence for platinum enrichment in depleted island-arc mantle sources. Geology 29, 851–854.
Kodolányi, J., Pettke, T., Spandler, C., Kamber, B.S., Gméling, K., 2012. Geochemistry of ocean floor and fore-arc serpentinites: constraints on the ultramafic input to subduction zones. J. Petrol. 53, 235–270.
Liu, C.-Z., Snow, J.E., Hellebrand, E., Brugmann, G., von der Handt, A., Buchl, A., Hofmann, A.W., 2008. Ancient, highly heterogeneous mantle beneath Gakkel Ridge, Arctic Ocean. Nature 452, 311–316.
Liu, C.-Z., Xu, Y., Wu, F.-Y., 2018. Limited recycling of crustal osmium in forearc mantle during slab dehydration. Geology 46, 239–242.
Lorand, J.-P., Luguet, A., 2016. Chalcophile and siderophile elements in mantle rocks: trace elements controlled by trace minerals. Rev. Mineral. Geochem. 81, 441–488.
Mankinen, E.A., Gromme, C.S., Williams, K.M., 1991. Concordant paleolatitudes from ophiolitic sequences in the northern California Coast Ranges, U.S.A. Tectonophysics 198, 1–21.
Mattinson, J.M., Hopson, C.A., 1992. U/Pb Ages of the Coast Range Ophiolite: A Critical Reevaluation Based on New High-Precision Pb/Pb Ages. American Association of Petroleum Geologists Bulletin.
McDonough, W.F., Sun, S.S., 1995. The composition of the Earth. Chem. Geol. 120, 223–253.
Meisel, T., Horan, M.F., 2016. Analytical methods for the highly siderophile elements. Rev. Mineral. Geochem. 81, 89–106.
Menzies, M., Blanchard, D., Jacobs, J., 1977. Rare earth and trace element geochemistry of metabasalts from the Point Sal ophiolite, California. Earth Planet. Sci. Lett. 37, 203–215.
Mungall, J.E., Brenan, J.M., 2014. Partitioning of platinum-group elements and Au between sulfide liquid and basalt and the origins of mantle-crust fractionation of the chalcophile elements. Geochim. Cosmochim. Acta 125, 265–289.
O'Driscoll, B., González-Jiménez, J.M., 2016. Petrogenesis of the platinum-group minerals. Rev. Mineral. Geochem. 81, 489–578.
O'Driscoll, B., Day, J.M.D., Walker, R.J., Daly, J.S., McDonough, W.F., Piccoli, P.M., 2012. Chemical heterogeneity in the upper mantle recorded by peridotites and chromitites from the Shetland Ophiolite complex, Scotland. Earth Planet. Sci. Lett. 333–334, 226–237.
O'Driscoll, B., Walker, R.J., Day, J.M.D., Ash, R.D., Daly, J.S., 2015. Generations of melt extraction, melt–rock interaction and high-temperature metasomatism preserved in peridotites of the ~497 Ma Leka Ophiolite Complex, Norway. J. Petrol. 56, 1797–1828.
O'Driscoll, B., Walker, R.J., Clay, P.L., Day, J.M.D., Ash, R.D., Daly, J.S., 2018. Length-scales of chemical and isotopic heterogeneity in the mantle section of the Shetland Ophiolite Complex, Scotland. Earth Planet. Sci. Lett. 488, 144–154.
Parkinson, I.J., Pearce, J.A., 1998. Peridotites from the Izu–Bonin–Mariana Forearc (ODP Leg 125): evidence for mantle melting and melt–mantle interaction in a supra-subduction zone setting. J. Petrol. 39, 1577–1618.
Parkinson, I.J., Hawkesworth, C.J., Cohen, A.S., 1998. Ancient mantle in a modern arc: osmium isotopes in Izu-Bonin-Mariana forearc peridotites. Science 281, 2011–2013.
Paulick, H., Bach, W., Godard, M., De Hoog, J.C.M., Suhr, G., Harvey, J., 2006. Geochemistry of abyssal peridotites (Mid-Atlantic Ridge, 15 20′ N, ODP Leg 209): implications for fluid/rock interaction in slow spreading environments. Chem. Geol. 234, 179–210.
Pearce, J.A., Parkinson, I.J., 1993. Trace element models for mantle melting: Application to volcanic arc petrogenesis. In: Prichard, H.M., Alabaster, T., Harris, N.B.W., Neary, C.R. (Eds.), Magmatic Processes and Plate Tectonics. Geological Society, London, Special Publications. 76. pp. 373–403.
Righter, K., Chesley, J.T., Ruiz, J., 2002. Genesis of primitive, arc-type basalt: Constraints from Re, Os, and Cl on the depth of melting and role of fluids. Geology 30, 619–622.
Saha, A., Basu, A.R., Jacobsen, S.B., Poreda, R.J., Yin, Q.Z., Yogodzinski, G.M., 2005. Slab devolatilization and Os and Pb mobility in the mantle wedge of the Kamchatka arc. Earth Planet. Sci. Lett. 236, 182–194.
Saleeby, J.B., Blake, M.C., Coleman, R.G., 1984. Pb/U zircon ages on thrust plates of west-central Klamath Mountains and Coast Ranges, northern California and southern Oregon. Eos (American Geophysical Union Transactions) 65, 1147.
Schulte, R.F., Schilling, M., Horan, M.F., Anma, R., Komiya, T., Farquhar, J., Piccoli, P.M., Pitcher, L., Walker, R.J., 2009. Chemical and chronologic complexity in the convecting upper mantle: evidence from the Taitao Ophiolite, southern Chile. Geochim. Cosmochim. Acta 73, 5793–5819.
Shervais, J.W., 1990. Island arc and ocean crust ophiolites: Contrasts in the petrology, geochemistry and tectonic style of ophiolite assemblages in the California Coast Ranges. In: Malpas, J. (Ed.), Ophiolites, Oceanic Crustal Analogues. Cyprus Geological Survey Department, Nicosia, pp. 507–520.
Shervais, J.W., Kimbrough, D.L., 1985. Geochemical evidence for the tectonic setting of the Coast Range ophiolite: a composite island-arc–oceanic crust terrane in western California. Geology 13, 35–38.
Shervais, J.W., Kimbrough, D.L., Renne, P., Hanan, B.B., Murchey, B., Snow, C.A., Zoglman Schuman, M.M., Beaman, J., 2004. Multi-stage origin of the Coast Range ophiolite, California: implications for the life cycle of supra-subduction zone ophiolites. Int. Geol. Rev. 46, 289–315.
Snortum, E., Day, J.M.D., Jackson, M.G., 2019. Pacific lithosphere evolution inferred from Aitutaki mantle xenoliths. J. Petrol. 60, 1753–1772.
Snow, J.E., Reisberg, L., 1995. Os isotopic systematics of the MORB mantle: results from altered abyssal peridotites. Earth Planet. Sci. Lett. 133, 411–421.
Stern, R.J., Bloomer, S.H., 1992. Subduction zone infancy: examples from the Eocene Izu-Bonin-Mariana and Jurassic California Arcs. GSA Bull. 104, 1621–1636.
Suhr, G., Seck, H.A., Shimizu, N., Günther, D., Jenner, G., 1998. Infiltration of refractory melts into the lowermost oceanic crust: evidence from dunite- and gabbro-hosted clinopyroxenes in the Bay of Islands Ophiolite. Contrib. Mineral. Petrol. 131, 136–154.
Sun, C., Liang, Y., 2014. An assessment of subsolidus re-equilibration on REE distribution among mantle minerals olivine, orthopyroxene, clinopyroxene, and garnet in peridotites. Chem. Geol. 372, 80–91.
Wakabayashi, J., 2017. Serpentinites and serpentinites: Variety of origins and emplacement mechanisms of serpentinite bodies in the California Cordillera. Island Arc 26, e12205.
Widom, E., Kepezhinskas, P., Defant, M., 2003. The nature of metasomatism in the sub-arc mantle wedge: evidence from Re-Os isotopes in Kamchatka peridotite xenoliths. Chem. Geol. 196, 283–306.
Workman, R.K., Hart, S.R., 2005. Major and trace element composition of the depleted MORB mantle (DMM). Earth Planet. Sci. Lett. 231, 53–72.
Xiong, Y., Wood, S.A., 2000. Experimental quantification of hydrothermal solubility of platinum-group elements with special reference to porphyry copper environments. Mineral. Petrol. 68, 1–28.